PHYSICAL REVIEW B **76**, 014202 (2007)

Structure-energy map of alkali borosilicate glasses: Effects of pressure and temperature

Lothar Wondraczek,[1,*] Sabyasachi Sen,[2] Harald Behrens,[3] and Randall E. Youngman[4]
[1]*Corning European Technology Center, Corning SAS, Avon, France*
[2]*Department of Chemical Engineering and Materials Science, University of California at Davis, Davis, California 95616, USA*
[3]*Leibniz University of Hannover, Hannover, Germany*
[4]*Corning Incorporated, Corning, New York 14831, USA*
(Received 16 March 2007; revised manuscript received 30 May 2007; published 11 July 2007)

A study of thermodynamic properties and structure of sodium borosilicate glasses with a range of pressure-temperature histories is presented. It is demonstrated how differences in the pressure-temperature path of the liquid during cooling may result in glasses with identical short-range structure and molar volume but different potential energies and, thus, different mid- or long-range structures. Rates of changes of molar volume, excess enthalpy, and boron coordination with changing fictive pressure and fictive temperature are reported. A structure-energy map is given, and paths for transitions under constant pressure, as well as between different pressures are shown. It is shown for pressures between atmospheric and 500 MPa that similar rates of cooling produce similar relative variations in fictive temperature in boron coordination environment and in the potential energy as compared to a given reference state. These results indicate that the rate of configurational entropy generation is independent of pressure in this range.

DOI: 10.1103/PhysRevB.76.014202 PACS number(s): 61.43.Fs, 64.70.Pf, 62.50.+p

I. INTRODUCTION

Pressure and temperature are important thermodynamic variables that determine the structure, dynamics, and macroscopic properties of a material. In the case of crystalline materials, pressure and temperature control the stability fields of different polymorphs of the same chemical composition. In this context, the question regarding the existence of thermodynamically distinct liquid or glassy phases of equivalent composition, i.e., the phenomenon of pressure-induced polyamorphism, became highly debated in recent years.[1] Polyamorphism has been suggested in multiple glass-forming materials, e.g., water,[2] elemental liquids,[3,4] metallic glasses,[5] and more complex systems.[6,7] However, while most existing literature is focused on the phenomenon as such, its nature and eventual generality are far from being understood. For geologic systems, the interest in the role of pressure on the structure and dynamics of glasses and liquids is obvious, as pressure increases toward the interior of the Earth and approaches already several gigapascals in the Earth mantle. However, technical relevance, as well, can be found in the regime of some hundreds of megapascals, e.g., in injection molding or pressure-assisted sintering. This intermediate regime of <1 GPa is twofold interesting for glasses: to study the onset of polyamorphic transitions in appropriate glass-forming systems and to draw conclusions for technically relevant materials. Such transitions can be described in the framework of energy landscapes.[8] Then, the energetic state of liquids may be described by two contributions: potential energy which may be expressed, for an isobaric transition, by a fictive temperature and kinetic energy, expressed by the real temperature. If the two temperatures decouple, then the liquid undercools and becomes a glass.[9] In nonisobaric transitions, fictive and real pressures become additional parameters.[10]

In this context, the term *apparent fictive temperature of a glass* was introduced to describe compression-induced contributions to the potential energy of glasses.[11,12] It was observed for a stoichiometric $CaMgSi_2O_6$ glass that quenching the starting liquid under pressure resulted in an additional endothermic effect during subsequent reheating under ambient pressure. The overshoot in the isobaric heat capacity C_p as observed by differential scanning calorimetry (DSC) in the glass transition range was found to depend on the pressure at which the glass was frozen in. The apparent fictive temperature determined at ambient pressure thus describes the fictive enthalpic equilibrium between a compressed glass and its corresponding melt, if the melt is under ambient pressure. It was suggested that from the apparent fictive temperature, a formal "equivalent cooling rate" can be extracted—the cooling rate which is required to reach equivalent potential energy in an uncompressed glass. However, direct comparative studies are needed in order to experimentally establish the structural and energetic relationship between the equivalent cooling rate induced by pressure and real cooling rates during glass transition. In this paper, we present the recent results of a thermodynamic and structural study of alkali borosilicate glasses derived from its parent liquid by cooling at different rates and under different pressures. A structure-energy map for this glass-forming system is derived on the basis of these results, and the nature of the relationship between the potential energy, structure, and kinetic energy is addressed.

II. EXPERIMENT

Alkali borosilicate glasses are well studied systems with respect to structure and associated properties. Boron coordination in those systems is well known to depend not only on composition,[13] but also on thermal history.[14,15] Increasing boron coordination at pressures of several gigapascals has also been evidenced in both boria[16] and borosilicates.[17] Here, a model system of composition (mol. %) $16Na_2O$-$10B_2O_3$-$74SiO_2$ was employed because of its stability against phase separation under the considered experimental conditions and because it is representative of many technologically relevant glasses.

A. Sample preparation and compression experiments

The Na-borosilicate glass was synthesized at the Federal Institute of Materials Testing (BAM, Berlin, Germany) from a batch of 3500 *g* of sodium carbonate, quartz, and boric acid. The batch was inductively melted and stirred for 1 h at 1400 °C in a platinum crucible, cast into preheated molds, and slowly cooled to room temperature. The glass thus obtained was transparent, stress-free, and free of crystals. Infrared (IR) absorption spectra were recorded using an IR microscope (Bruker IRscopeII) equipped with a Fourier transform IR spectrometer (Bruker IFS88). Water content of the glass was determined from the peak height of the absorption band at $3550\ \mathrm{cm}^{-1}$ using a calibrated absorption coefficient of $5.52 \pm 0.28\ \mathrm{m}^2\ \mathrm{mol}^{-1}$. This absorption coefficient was experimentally determined for this composition using a set of hydrous glasses for which the water content was measured by Karl-Fischer titration. An average water content of 153 ± 8 ppm by weight was obtained for 95 analyses of the glass. The chemical composition of all samples was systematically verified throughout the study by energy dispersive x-ray analysis and comparison to reference data.

Glass samples were quenched from high pressures at well-controlled cooling rates in order to be able to separate thermal and pressure-induced effects. To access the onset of pressure-induced structural alterations of the system, experiments were carried out in the intermediate pressure regime, i.e., <1 GPa, which also enabled the use of large samples.

Individual sample rods ($4 \times 4 \times 25\ \mathrm{mm}^3$) were cut from one large (~1.5 kg) bar to guarantee sample homogeneity. Compression experiments were performed at pressures of up to 500 MPa in a cold seal pressure vessel. The rods were loaded directly into the vessel, and argon gas was employed as the compression medium. The samples were equilibrated at temperatures between 861 and 889 K for ~10 min. Considering a dilatometric glass transition temperature T_g of ~853 K,[26] the equilibration time in these high-pressure–high-temperature experiments was well above the relaxation time of the glass and/or liquid. Temperature was recorded continuously with a NiCr-Ni thermocouple in a bore hole at the end of the autoclave. Temperature at the sample position (accuracy of ±5 K) was calibrated under pressure in a separate run using three NiCr-Ni thermocouples that were inserted into the autoclave. Pressure was held constant with an automatic pumping system and was measured with a strain gauge manometer (accuracy of ±5 MPa). Glasses were cooled under pressure by switching off the furnace. Cooling rates for these experiments vary in the range of $(3.6-4.6) \pm 0.2$ K/min at temperatures down to 730 K and <3 K/min down to room temperature. One sample, compressed at 500 MPa, was quenched significantly faster (~40 K/min) by pulling the autoclave out of the furnace. Density of each sample was determined by helium pycnometry. Compressed samples were polished (silicon carbide and ethanol) on all sides, removing ~150 μm of the surface to avoid any interference from surface alteration or diffusion (during compression, samples were in direct contact with the compression medium argon and eventual atmospheric impurities that might diffuse into the glass). Subsequently, disks of ~1 mm thickness were broken from each bar and used for DSC and nuclear magnetic resonance (NMR) spectroscopy. An additional set of samples was produced by equilibrating at ambient pressure and 930 K and cooling at rates of 0.3, 3, 20, and ~400 K/min (while low and intermediate cooling rates were carefully controlled to within ±0.2 K/min, the rate of 400 K/min was estimated for fast cooling in air by letting a 70 mg specimen fall out of a vertical tube furnace).

B. DSC measurements

DSC measurements were conducted with a scanning calorimeter (Netzsch DSC 404 C) under nitrogen atmosphere at ambient pressure. Temperature and sensitivity calibrations were performed systematically with benzoic acid, silver sulfate, cesium chloride, and barium carbonate references. At the beginning of each scan, the system was equilibrated at 473 K for 15 min, then heated to 950 K at 20 K/min, equilibrated for 5 min, and then cooled back to 473 K. DSC cooling rates after first and second scans were 3 K/min for the compressed samples, slightly lower than the cooling rate at which the samples were quenched under high pressure. The corresponding DSC cooling rate for the noncompressed samples was 20 K/min. For every experiment, four scans were performed in sequence: base line (empty crucible), reference (sapphire, 55.6 mg), and first and second scans of the actual sample [~1 mm thick sample disks, $(40-60) \pm 0.05$ mg]. To enable optimum heat transfer, employed sample disks were polished a second time on the face that was in contact with the bottom of the crucible used in the DSC experiments. No mass loss was detected after the DSC experiments.

C. NMR spectroscopy

^{11}B magic-angle-spinning (MAS) NMR spectra of the glass samples were obtained using a commercial spectrometer (Chemagnetics/Varian) in conjunction with an 11.7 T wide bore superconducting magnet. At this field strength, the resonance frequency of ^{11}B is 160.3 MHz. Finely crushed glass samples of ~150 mg were loaded into 3.2 mm zirconia rotors and spun at 20 kHz. Spectra were collected with a 3.2 mm double resonance T3 probe (Varian). To maintain accurate relative intensities of the trigonal and tetrahedral boron resonances, very short pulse widths of 0.6 μs (approximately $\pi/12$) and recycle delays of 2 s were utilized. 2048 transients were averaged together and Fourier transformed without additional line broadening to obtain each spectrum. The ^{11}B NMR spectra were referenced to an external shift standard of BF_3-Et_2O at 0 ppm.

III. RESULTS AND DISCUSSION

The pressure-temperature-time history of the glass samples at various stages of the experiment is schematically shown in Fig. 1. After equilibrating at high temperature and

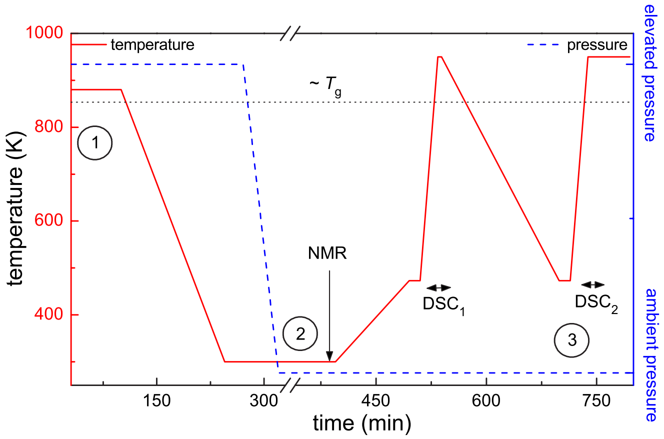

FIG. 1. (Color online) Schematic of the performed experiments: samples were initially (1) equilibrated under high pressure, above their glass transition temperature T_g, subsequently cooled under pressure, and subjected to NMR analysis (2). This was followed by the first DSC scan, during which samples recovered to state (3) and a final reference DSC scan.

high pressure, a melt at stage (1) is quenched under pressure at a certain cooling rate q_1, resulting in a glass at state (2). During compression, the glass inelastically densifies, as was quantified by density measurements under ambient pressure (Fig. 2). The densified glass is then subjected to NMR analysis and, subsequently, the first DSC up scan under ambient pressure and at a heating rate q_2, during which compression is released. After that up scan, the sample is cooled at a rate equivalent to q_1, but under ambient pressure, to arrive at stage (3). Finally, a second up scan is performed, once again at q_2, during which only relaxation or recovery occurs, while no change in internal pressure takes place. Consequently, the second DSC up scan of each sample represents a reference state with respect to ambient pressure, and it is represented by a fictive temperature determined only by q_1. The fact that these second up scans for all samples are indistinguishable from one another within the limits of experimental errors (inset of Fig. 3) indicates that during cycling the sample, no undesired side effects such as crystallization, evaporation of glass components, or phase separation occurred to an extent that would disturb further interpretation of the data. X-ray diffraction and scanning electron microscopy of these samples at the end of the experimental runs corroborate with this conclusion.

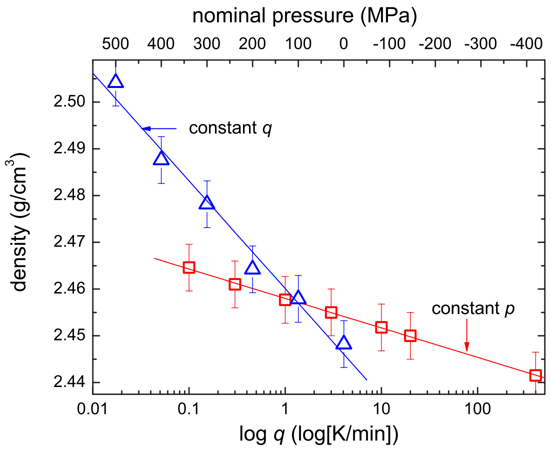

FIG. 2. (Color online) Density ρ of compressed glasses for different pressures (triangles) and noncompressed glasses for different cooling rates (squares) as measured under ambient pressure. Lines: linear regressions: $\rho=2.447\ \mathrm{g/cm^3}+[1.094\times10^{-4}\ \mathrm{g/(cm^3\ MPa)}]\times p$, $r=0.991$ for glasses that were cooled under pressure at constant cooling rate, and $\rho=2.458\ \mathrm{g/cm^3}-\{6.3\times10^{-3}\ \mathrm{g/[cm^3\ log(K/min)]}\}\times\log q(\mathrm{K/min})$. Lines correspond to linear regressions of density (in $\mathrm{g/cm^3}$) as function of pressure (in MPa) or cooling rate in (K/min): $\rho=2.447+(1.094\times10^{-4})\times p$, $r=0.991$, and $\rho=2.458-(6.3\times10^{-3})\times\log q$, $r=0.999$.

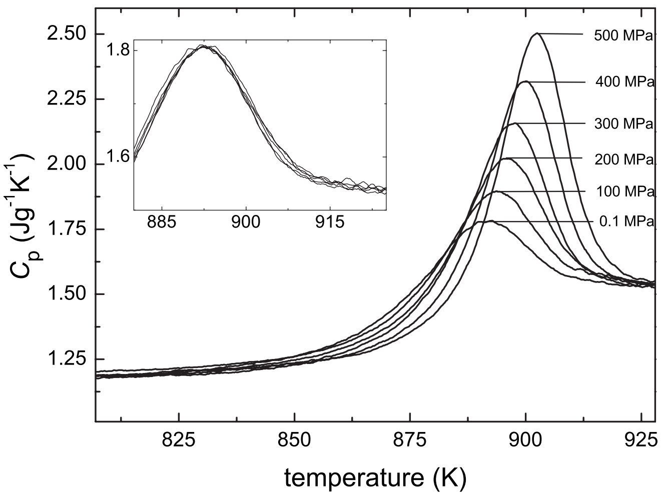

FIG. 3. Evolution of the endothermic overshoot in isobaric heat capacity close to the glass transition temperature with changing nominal pressure. DSC scans were performed at ambient pressure. Inset: Second DSC scans of all samples after recovery during the first scan.

Glass transition ranges as observed during the first DSC up scans for samples that were compressed in their melt state are shown in Fig. 3. The clearly visible overshoot in isobaric heat capacity C_p is generally considered a direct consequence of the nonlinearity of the relaxation process,[18] i.e., the result of a broadening in the distribution function of relaxation times. Typically, the overshoot and, hence, the nonlinearity of enthalpy relaxation during the up scan increase with decreasing cooling rate of the melt. In the present experiments, this overshoot also depends on the extent of compression recovery of the glass. A characteristic temperature T_f can be found for the glass that describes its fictive enthalpy equilibrium with the corresponding liquid[19] and, hence, its potential energy that satisfies the relation

$$\int_{T_0}^{T_f}(C_{pl}-C_{pg})dT' = \int_{T_0}^{T}(C_p-C_{pg})dT', \tag{1}$$

with T_0 being a temperature well above the glass transition temperature, T a temperature well below, and C_{pl}, C_{pg}, and C_p the isobaric heat capacities of the liquid, the glass (extrapolated to T or T_0, respectively), and as measured. For the isobaric case, this characteristic temperature is the *fictive*

TABLE I. Properties of examined glasses after compression and/or slow cooling.

Generic pressure (MPa)	First cooling rate ($K\ min^{-1}$)	T_f[a] (± 2 K)	Density (± 0.005 $g\ cm^{-3}$)	$[BO_4]$ ($\pm 0.5\%$)	ln K	T_{f0}[b] (± 8 K)	Second cooling rate (± 0.2 $K\ min^{-1}$)	T_f[c] (± 2 K)
0.1	4.6±0.2	843	2.448	89.3	2.122	843	3	841
100	3.8±0.2	839	2.458	89.9	2.186	851	3	843
200	3.7±0.2	833	2.464	91.8	2.415	858	3	843
300	4.2±0.2	831	2.478	92.2	2.470	868	3	843
400	3.6±0.2	827	2.488	93.0	2.587	875	3	842
500	4.5±0.2	821	2.504	94.2	2.788	881	3	843
500	40±0.5	843	2.484	93.1	2.602	905	10	852
0.1	0.3±0.2	825	2.461	90.1	2.208		20	854
0.1	3±0.2	842	2.455	89.5	2.143		20	855
0.1	20±0.2	854	2.450	88.8	2.070		20	854
0.1	400±10	880	2.442	87.2	1.919		20	854

[a] After first cooling; T_{fA} for pressures >0.1 MPa and T_{f0} for 0.1 MPa, analytically determined from Eq. (1), using first DSC up scan (up scan rate: 20 K/min).

[b] After first cooling; estimated for compressed samples from Eq. (5).

[c] After second cooling; T_{f0}.

temperature T_{f0}, while in the presence of changes in internal pressure, it is the apparent fictive temperature T_{fA}.[11] The values of T_f that were determined analytically from Eq. (1) are given in Table I.

It is clear from Fig. 4 that T_{fA} and T_{f0}, representing constant cooling rate and constant pressure, respectively, can be translated into each other when the reciprocal of the former $(1/T_f)$ is plotted as a linear function of pressure p and the latter is plotted as a logarithmic function of cooling rate q. It has been shown in previous studies[19] that $d \log q / d(1/T_f) = -\Delta h^* / R$, where Δh^* is the activation energy of the relaxation time scale in the glass (or of shear relaxation) in the temperature region near the glass transition and R is the universal gas constant. This relationship explains the negative slope of $\log q$ vs $1/T_f$ for the ambient-pressure experiments in Fig. 4. On the other hand, it has been shown in a recent study[20] that the boron speciation reaction that controls the volume of the glass can be written as

$$BO_4 \leftrightarrow BO_3 + NBO. \tag{2}$$

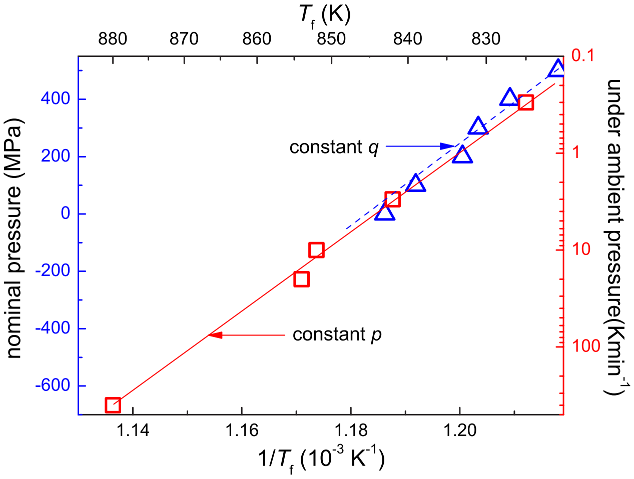

FIG. 4. (Color online) Fictive temperatures of compressed samples (T_{fA}, triangles) and samples that were cooled at different rates under ambient pressure (T_{f0}, squares). Lines are guides for the eyes.

This equation describes the equilibrium between the total fractions of BO_4 groups, BO_3 groups, and nonbridging oxygens (NBO).

Equation (2) shifts to the right with increasing T_f and decreasing pressure.[20] For an initially fully polymerized glass, the equilibrium constant K for the formation of $[BO_4]$ is then given by Eq. (3):

$$K = \frac{[BO_4]}{NBO \cdot [BO_3]} = \frac{[BO_4]}{(100 - [BO_4])^2}. \tag{3}$$

As in the glass that was used for the present study, the molar content of Na_2O strongly exceeds that of B_2O_3, and the variation in BO_4 is relatively small (but structurally significant); the concentration of NBO, in a first approximation, can be assumed constant and the equilibrium constant K for the reaction can be written as

$$K = \frac{[BO_4]}{100 - [BO_4]}, \tag{4}$$

where brackets indicate the mole percentage of BO_4 and BO_3.

It is assumed that this reaction is also primarily responsible for the generation of nearly all of the configurational entropy in borate and borosilicate glasses in the glass transi-

TABLE II. Experimentally determined rates of compaction, enthalpy generation, and $[\mathrm{BO_4}]$ speciation dependent on pressure of freezing and cooling rates, expressed by the isobaric fictive temperature T_{f0}.

$dV/dp\vert_q$ ($\mathrm{m^3\,mol^{-1}\,MPa^{-1}}$)	$dV/dT_f\vert_{p=0.1\ \mathrm{MPa}}$ ($\mathrm{m^3\,mol^{-1}\,K^{-1}}$)	$\frac{d(\Delta H_{ex})}{dp}\vert_q$ ($\mathrm{J\,g^{-1}\,MPa^{-1}}$)	$\frac{d(\Delta H_{ex})}{dT_f}\vert_{p=0.1\ \mathrm{MPa}}$ ($\mathrm{J\,g^{-1}\,K^{-1}}$)	$\frac{d(\ln K)}{dp}\vert_q$ ($\mathrm{MPa^{-1}}$)	$\frac{d(\ln K)}{dT_f}\vert_{p=0.1\ \mathrm{MPa}}$ ($\mathrm{K^{-1}}$)
-1.1×10^{-9}	3.75×10^{-9}	0.023	−0.185	1.31×10^{-3}	-5.36×10^{-3}

tion range. The temperature dependence of the equilibrium constant K for this reaction is given by the van't Hoff relation

$$\Delta H = -R\left[\frac{\ln K_1-\ln K_2}{\frac{1}{T_1}-\frac{1}{T_2}}\right]. \tag{5}$$

In this expression, ΔH is the enthalpy change associated with the speciation reaction, R is the gas constant, and K_1 and K_2 are the equilibrium constants for the reaction at two different temperatures T_1 and T_2. According to the Adam-Gibbs theory, the temperature dependence of the configurational entropy controls the activation energy of the relaxation time scale.[21] Therefore, considering the simple thermodynamic relationships between enthalpy, temperature, heat capacity, and entropy, it can be shown that $\Delta H=\Delta h^*$ and hence,

$$d\ln K/d(1/T_f) = -\Delta h^*/R. \tag{6}$$

Previous spectroscopic studies have suggested that pressure dependent volume change in borosilicate glasses near glass transition is driven by the same borate speciation reaction *but in opposite direction*.[17] In that case, according to classical thermodynamics,

$$\Delta V/RT = d\ln K/dP. \tag{7}$$

Combining Eqs. (6) and (7), one finally obtains the relation

$$dP/d(1/T_f) = -\Delta h^* T/\Delta V. \tag{8}$$

Pressure-induced densification of the glass results in negative ΔV (Fig. 2), and therefore, this relationship implies a positive slope of pressure vs $1/T_f$, as observed in Fig. 4.

Combining the measured density (Fig. 2, Table I) with the molar mass of the glass of ~61.6 g/mol, one can directly calculate the rates of compaction as function of pressure and cooling rate. While the former yields the molar rate of compression for constant cooling rates $dV/dp|_q$, the latter, if expressed as $dV/dT_{f0}|_{p=0.1\ \mathrm{MPa}}$, is a measure of thermal expansion in the glass transition range. Derived values are given in Table II and will be considered later.

The observation of the equivalence of the variation of fictive temperature with pressure at a constant cooling rate and with cooling rate at ambient pressure is rather intriguing (Fig. 4). This result clearly implies that compressing and quenching a melt at a given pressure may result in a glass with the same potential energy as if it was cooled at a much slower rate under lower pressure.[11] For instance, in the present experiment, equivalent potential energies were found for glasses that were equilibrated and quenched either at 400 MPa and 4 K/min or at 0.1 MPa and 0.3 K/min. An important question that might arise in relation to polyamorphism and in the potential energy landscape scenario of relaxation is whether structurally and energetically equivalent glasses can be derived from the melt via separate pressure-temperature-time paths.

As mentioned before, boron coordination in a borosilicate glass is sensitive to its fictive temperature as well as to generic pressure[14–17] to an extent that can readily be detected by NMR. The ratio of tetrahedrally and trigonally coordinated B atoms ($\mathrm{BO_4:BO_3}$) in the glass structure is expected to increase with decreasing fictive temperature and increasing pressure. ^{11}B MAS NMR can thus be used to access the short-structural response of the glass to different cooling rates and to compression. A comparison of fraction of tetrahedrally coordinated boron in samples that were cooled from above their glass transition temperature at different rates under ambient pressure, and in samples that were cooled under different pressures at a constant rate, evidently indicates decoupling between the two paths (Fig. 5, Table I).

With these data, the equilibrium constant can be calculated from Eq. (4) for different pressures during freezing and different cooling rates. Plotting $\ln K$ [Eq. (4) and Table I] versus p (for compressed glasses) and T_{f0}, respectively, also yields linear dependences with the slopes being the rates of pressure and, respectively, cooling rate—induced changes in boron speciation (Fig. 6). Rates $d\ln K/dp|_q$ and $d\ln K/dT_{f0}|_{p=0.1\ \mathrm{MPa}}$ are given in Table II.

The difference in the slopes of pressure and temperature dependences of boron coordination environments in Fig. 5 can now be simply understood assuming that the boron speciation reaction controls the temperature and pressure dependent volume changes in the system (*vide supra*). The correlation between both properties becomes evident when comparing the rates of molar volume changes to the rates of changes in $\ln K$: the ratios

$$d\ln K/dp|_q : d\ln K/dT_{f0}|_{p=0.1\ \mathrm{MPa}} \sim 0.25$$

and

$$dV/dp|_q : dV/dT_{f0}|_{p=0.1\ \mathrm{MPa}} \sim 0.3$$

are, within experimental errors, equivalent. Hence, the two distinct slopes in Fig. 5 correspond to differences in pressure and temperature dependences of volume and are measures of compressibility and thermal expansivity, respectively, as noted before. From extrapolation of the curves, it can be estimated that, formally, to achieve the same amount of $\mathrm{BO_4}$ groups as is found after compression at 400 MPa, a cooling rate of $\sim10^{-4}$ K/min would be necessary under ambient pressure. The resulting slowly cooled glass (cooling would

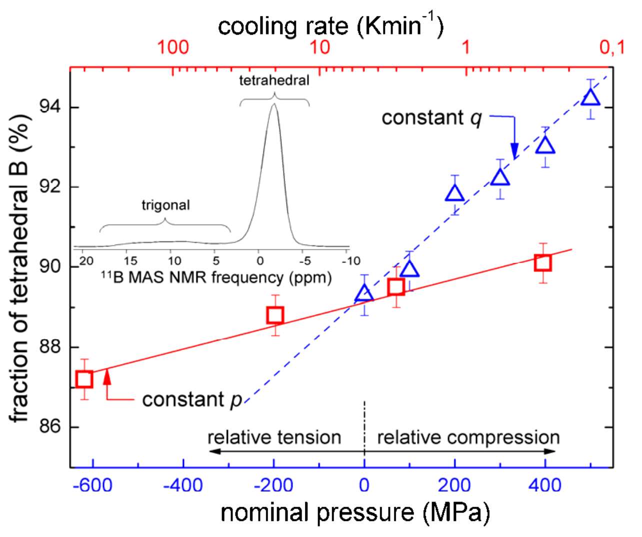

FIG. 5. (Color online) Fraction of B atoms present as BO_4 units as observed by ^{11}B MAS NMR spectroscopy for samples that were frozen in under elevated pressure (cooling rate of 4±0.5 K/min, triangles) and frozen in under ambient pressure but at different cooling rates (squares), respectively. Inset: exemplary NMR spectrum (500 MPa and 4±0.5 K/min). On the pressure axis, positive values correspond to compression, and negative values result from extrapolation of the data and correspond to tension relative to the reference pressure (ambient).

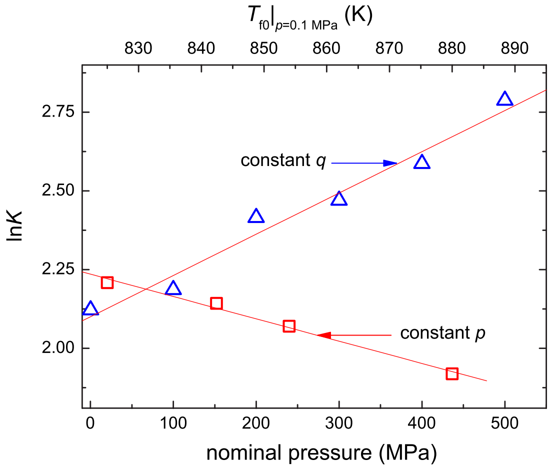

FIG. 6. (Color online) Dependence of equilibrium constant *K* of the B-speciation reaction [Eq. (2)] on pressure of freezing (triangles) and cooling rate (squares), expressed as the isobaric fictive temperature.

require more than five years) would possess not only the same amount of BO_4 goups but also the same molar volume. However, its fictive temperature $T_{f0} \sim 770$ K (extrapolation of data from Fig. 4) would significantly differ from that of the compressed glass ($T_{fA}=825$ K). Note that in Figs. 4 and 5, the same scaling was used for p and q, i.e., $\log q(\text{K/min}) \rightarrow 0.67 - p(\text{MPa})/330$. This scaling is arbitrary in the sense that it was chosen only to illustrate how structure and potential energy evolve differently.

The rate of enthalpy of formation with changing pressure of freezing or changing cooling rate can be quantified by considering the evolution of excess enthalpy, as can be derived by integrating the endothermic overshoot in the DSC curves.[12,22] The derived values of $d(\Delta H)/dp|_q$ and $d(\Delta H)/dT_{f0}|_{p=0.1\text{ MPa}}$ are given in Table II (for the relatively small changes in fictive temperature, a linear dependence of excess enthalpy on T_{f0} is assumed). Here, the ratio of pressure and temperature dependent rates is 0.13. This small value (as compared to volume and coordination changes) clearly indicates that the reaction that governs changes in molar volume and boron coordination is not the sole reason for enthalpy changes, as well.

In Fig. 7, the respective ^{11}B NMR data are plotted versus the fictive temperatures T_{fA} and T_{f0}, respectively. Figure 7 can be considered as a structure-energy map of the employed borosilicate glass: while fraction of BO_4 is clearly a representative structural parameter, T_f directly reflects the potential energy of the system. Although represented only by two points, Fig. 7 shows a second isobar for compression and freezing at 500 MPa in the range 4–40 K/min. A linear regression of those two points yields a slope equivalent to that of the isobar for ambient-pressure experiments. This implies that the response of structure to *changes* in isobaric T_{f0} is independent of pressure. Considering the already discussed equivalence of changes in $[BO_4]$ and molar volume, it also reflects that the thermal expansion is practically independent of pressure in the observed regime. Furthermore, two trends are illustrated in Fig. 7 for constant cooling and varying pressure. The trend for a cooling rate of 4.0±0.5 K/min is well established by the experimental data. The second line for 40 K/min was constructed by combining experimental data from a high-pressure experiment at 40 K/min (500 MPa) with the estimate of T_{f0} (40 K/min, 0.1 MPa) $=861\pm4$ K/min and BO_4 fraction$=0.881\pm0.005$. This esti-

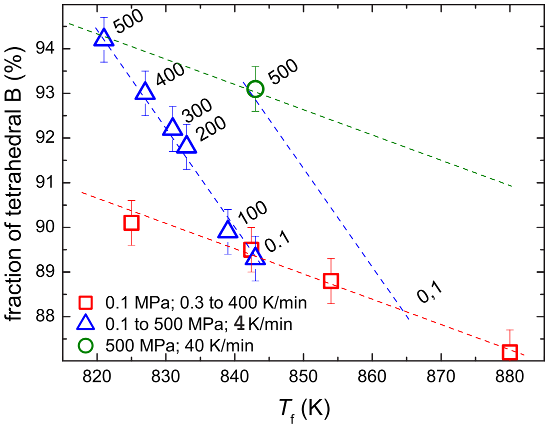

FIG. 7. (Color online) Structure-energy map of the studied borosilicate glass: T_f directly reflects potential energy (T_{f0} for noncompressed glasses, squares; T_{fA} for compressed glasses, triangles and circle), and the fraction of tetrahedrally oriented boron is a characteristic structural parameter. Parallel dashed lines (guides for the eyes) indicate isobaric levels at 0.1 and 500 MPa, respectively, for different cooling rates; dotted lines indicate transitions between those levels at given cooling rates of 3 and 40 K/min, respectively, for changing pressures. Labels: Pressure in MPa.

mate was derived from Figs. 4 and 5: interpolation of Fig. 4 yields T_{f0} for ambient-pressure cooling at 40 K/min, and interpolation of Fig. 5 yields the corresponding $[\mathrm{BO_4}]$ data. In a first approximation, both trends are parallel (dashed lines). Moreover, any horizontal line in this plot would intersect the $[\mathrm{BO_4}]$-T_f isobars at several points, indicating that same short-range structure can be produced via a variety of combinations of pressures and cooling rates.

As shown previously,[11] T_{f0} for compressed glasses can be estimated from Eq. (9) with the help of classical thermodynamics:

$$T_{f0} = T_{fA}\left[1 + \frac{V(p_0 - p)(\alpha_{Vl} - \alpha_{Vg})}{C_{pl} - C_{pg}}\right], \tag{9}$$

where α_{Vl} and α_{Vg} are the volumetric thermal expansion coefficients of the liquid and the glass, respectively, p_0 is a reference pressure (ambient), and V is the molar volume. This equation generally suggests a positive dependence between pressure and T_{f0}. Direct evidence for increasing T_{f0} with increasing pressure is available for organic glasses (e.g., Ref. 23). In the present case, for a rough estimate of T_{f0}, V can be calculated from the molar mass (~61.6 g/mol) and density values as given in Table I. Difference $C_{pl}-C_{pg}$ is ~20.3 J $(\mathrm{mol\,K})^{-1}$ using the DSC data in Fig. 3, and $\alpha_{Vl} - \alpha_{Vg} \sim 1.25 \times 10^{-4}\ \mathrm{K}^{-1}$. Here, the pressure dependence of α_V as well as temperature dependence of C_{pg} are neglected as described in Ref. 11. The largest uncertainty arises from the thermal expansion α_{Vl}. The employed value is the quotient of the experimentally determined rate of molar volume generation with changing fictive temperature (Table II) and the molar volume. This yielded a value of $\alpha_{Vl} \sim 1.5 \times 10^{-4}\ \mathrm{K}^{-1}$, whereas for α_{Vg}, a value of 0.25×10^{-4} was found in standard dilatometric experiments. Based on these parameters, values for T_{f0} were calculated as given in Table I. Those calculated values, in principle, indicate the fictive temperature that would be found if DSC experiments would be performed under pressure. The difference between T_{f0} and T_{fA} for a given cooling rate thus represents the pressure-induced change in potential energy of the glass. In a first approximation, boron coordination varies linearly with ΔT_f, as is shown in Fig. 8. Similarly, the difference in T_{f0} for different cooling rates, at ambient pressure, stands for the change in potential energy between differently cooled glasses. Calculating this difference for a given reference cooling rate (and, thus, reference fictive temperature) and relating it to boron coordination also yield a linear dependence with the same slope as for the compressed glasses. Indeed, if similar reference cooling rates are chosen (4 K/min for compressed glasses; 3 K/min for noncompressed glasses), both lines collapse together. Consequently, this indicates that changes in fictive temperature as compared to given reference conditions have an effect on boron coordination that is independent of whether those changes were produced by compression or different cooling rates. For example, cooling under 400 MPa at 4 K/min results in $\Delta T_f \sim -48$ K (Table I) during a recovery experiment at ambient pressure $(\Delta T_f = T_{f0} - T_{fA})$. A cooling rate of $\sim 10^{-4}$ K/min would have to be applied to lower T_f of a noncompressed sample, cooled at 4 K/min, by the same amount, e.g., from 843 to ~790 K (Fig. 3, Table I). The resulting fraction of $\mathrm{BO_4}$ would correspond to that found in the compressed glass. These results clearly indicate that generation of configurational entropy as a function of temperature is independent of pressure and therefore imply that the fragility of these glass-forming liquids would also be independent of pressure in this pressure range.

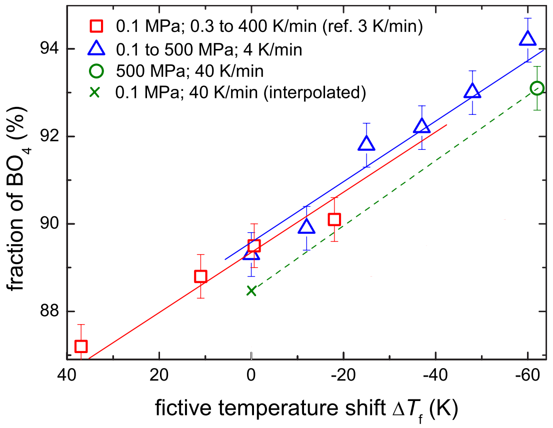

FIG. 8. (Color online) Fraction of $\mathrm{BO_4}$ versus compression and/or cooling-induced shift in T_f. For the compressed samples (triangles and circle), "shift" (ΔT_f) refers to the difference in T_{fA} and calculated T_{f0} (Table I), i.e., the contribution of compression recovery to potential energy for samples that were cooled at a given cooling rate. For noncompressed samples, the shift originates from variation in cooling rates, i.e., the difference between T_{f0} and T_{f0}^{ref}, where T_{f0}^{ref} is 843 K (3 K/min, squares). Lines are guides for the eyes.

Finally, with the derived data and assuming that the boron speciation in the glasses represents the equilibrium speciation in the melt at the fictive temperature T_{f0} (as found, for instance, for $\mathrm{H_2O}$ speciation in hydrous glasses,[24,25]) thermodynamic data for boron speciation in the borosilicate melts can be derived directly. The equilibrium constant for the reaction is related to the reaction enthalpy ΔH, the reaction entropy ΔS, and the reaction volume ΔV by

$$\ln K = -\frac{\Delta H}{RT} + \frac{\Delta S}{R} + \frac{\Delta V \cdot P}{RT}. \tag{10}$$

Since T_{f0} are best constrained for the 0.1 MPa data, we used these data first to calculate ΔH to be $-74.4 \pm 4.8\ \mathrm{kJ\,mol^{-1}}$ and ΔS to be $-47.6 \pm 4.8\ \mathrm{J\,mol^{-1}\,K^{-1}}$. Next, all data (including the high-pressure data) were fitted to Eq. (10) using the ΔH and ΔS from the ambient-pressure data as constraints. Thus, we obtained a reaction volume of $47.6 \pm 0.6\ \mathrm{cm^3\,mol^{-1}}$. These values reproduce the experimental $\ln K$ data with a root mean square deviation of 0.029.

IV. CONCLUSIONS

^{11}B MAS NMR and DSC analyses of alkali borosilicate melts that were quenched under different pressures and different cooling rates were performed *ex situ*. It was evidenced that changes in molar volume and short-range structure are governed by the same speciation reaction in compression as well as in cooling experiments, and thermodynamic data for this reaction are provided.

For pressures between atmospheric and 500 MPa, similar rates of cooling produce similar relative variations in boron coordination environment, which indicates that the rate of configurational entropy generation is virtually independent of pressure. Furthermore, for the examined glass, changes in fictive temperature and, thus, potential energy as compared to a given reference state have an effect on boron coordination that is independent of whether those changes were produced by compression or by different cooling rates.

In the present case, for example, *equivalent glasses* in the sense of equivalent fraction of BO_4 groups and molar volume possibly refer to the conditions 400 MPa and 4 K/min and 0.1 MPa and 10^{-4} K/min. However, the energetic equivalence of these two conditions depends on the point of reference, which needs to be at the respective levels of pressures. If two glasses are compared with respect to different reference pressures, their short-range structure can very well be alike, but their potential energies will differ, as was evidenced by the found rates of generation of excess enthalpy. While potential energy, on the other hand, directly reflects structure, this clearly indicates that equivalent boron coordination and equivalent molar volume can be found in different mid- or long-range configurations.

ACKNOWLEDGMENT

The authors wish to thank S. Reinsch, Federal Institute of Materials Testing, BAM, Berlin, Germany, for providing the employed base glass and corresponding standard data.

---

*wondraczl@corning.com

[1] P. H. Poole, C. A. Angell, T. Grande, and P. F. McMillan, Science **275**, 322 (1997).

[2] O. Mishima, L. D. Calvert, and E. Whalley, Nature (London) **314**, 76 (1985).

[3] S. K. Deb, M. Wilding, M. Somayazulu, and P. F. McMillan, Nature (London) **414**, 528 (2001).

[4] Y. Katayama, T. Mizutani, W. Utsumi, O. Shimomura, M. Yamakata, and K. Funakoshi, Nature (London) **403**, 170 (2000).

[5] H. W. Sheng, H. Z. Liu, Y. Q. Cheng, J. Wen, P. L. Lee, W. K. Luo, S. D. Shastri, and E. Ma, Nat. Mater. **6**, 192 (2007).

[6] S. Aasland and P. F. McMillan, Nature (London) **369**, 633 (1994).

[7] S. Sen, S. Gaudio, B. G. Aitken, and C. E. Lesher, Phys. Rev. Lett. **97**, 025504 (2006).

[8] F. H. Stillinger and T. A. Weber, Science **228**, 983 (1984); F. H. Stillinger, *ibid.* **267**, 1935 (1995); S. Sastry, P. G. Debenedetti, and F. H. Stillinger, Nature (London) **393**, 554 (1998).

[9] C. A. Angell, Y. Z. Yue, L. M. Wang, J. R. D. Copley, S. Borick, and S. Mossa, J. Phys.: Condens. Matter **15**, S1051 (2003).

[10] P. Gupta, J. Non-Cryst. Solids **102**, 231 (1988).

[11] L. Wondraczek, H. Behrens, Y. Z. Yue, J. Deubener, and G. W. Scherer, J. Am. Ceram. Soc. **90**, 1556 (2007).

[12] Y. Yue, L. Wondraczek, H. Behrens, and J. Deubener, J. Chem. Phys. **126**, 144902 (2007).

[13] W. J. Dell, P. J. Bray, and Z. Xiao, J. Non-Cryst. Solids **58**, 1 (1983).

[14] S. Sen, Z. Xu, and J. F. Stebbins, J. Non-Cryst. Solids **226**, 29 (1998).

[15] T. J. Kiczenski and J. F. Stebbins, Rev. Sci. Instrum. **77**, 013901 (2006).

[16] S. K. Lee, K. Mibe, Y. W. Fei, G. D. Cody, and B. O. Mysen, Phys. Rev. Lett. **94**, 165507 (2005).

[17] L.-S. Du, J. R. Allwardt, B. C. Schmidt, and J. F. Stebbins, J. Non-Cryst. Solids **337**, 196 (2004).

[18] I. M. Hodge, J. Non-Cryst. Solids **169**, 211 (1994).

[19] G. W. Scherer, *Relaxation in Glass and Composites* (Wiley-Interscience, New York, 1986).

[20] S. Sen, T. Topping, P. Yu, and R. E. Youngman, Phys. Rev. B **75**, 094203 (2007).

[21] G. Adam and J. H. Gibbs, J. Chem. Phys. **43**, 139 (1965).

[22] B. Martin, Y. Yue, L. Wondraczek, and J. Deubener, Appl. Phys. Lett. **86**, 121917 (2005).

[23] T. Atake and C. A. Angell, J. Phys. Chem. **83**, 3218 (1979).

[24] Y. Zhang, J. Jenkins, and Z. Xu, Geochim. Cosmochim. Acta **61**, 2167 (1997).

[25] H. Behrens and M. Nowak, Phase Transitions **76**, 45 (2003).

[26] S. Reinsch (private communication).